RSC Advances

PAPER

View Article Online
View Journal | View Issue

Cite this: *RSC Adv.*, 2024, **14**, 31861

A rhodamine-based fluorescent probe bearing 8-hydroxyquinoline group for the highly selective detection of Hg^{2+} and its practical application in cell imaging†

Lei Zhang,[a] Jun Guo[b] and Qihua You *[c]

Received 23rd August 2024
Accepted 2nd October 2024

DOI: 10.1039/d4ra06115b

rsc.li/rsc-advances

A highly selective and sensitive fluorescent probe, **RHOQ**, was designed for the detection of Hg^{2+} by incorporating an 8-hydroxyquinoline moiety onto a rhodamine molecular platform with a suitable linker. In MeOH–Tris (20 mM, pH = 7.4, 1 : 9, v/v) buffer solution, **RHOQ** exhibited 550-fold fluorescence enhancement at 594 nm upon addition of Hg^{2+}, with a fast response and a low detection limit (9.67×10^{-8} M). The 1 : 1 binding mode of **RHOQ** with Hg^{2+} was established using Job's plot, UV-Vis, and fluorescence spectroscopic titration methods. Furthermore, **RHOQ** was successfully applied for the detection of Hg^{2+} in living cells with good membrane permeability.

1 Introduction

The mercury ion is a highly toxic heavy metal that poses severe health risks to humans and wildlife. It is a global environmental pollutant that can enter the food chain through various sources, including industrial activities, mining, and natural processes. Mercury ions can accumulate in the body and cause various health issues, such as neurological disorders, kidney damage, and cardiovascular diseases. When inorganic Hg^{2+} entered living organisms, it would transform to lipophilic and higher toxic methylmercury (CH_3Hg^+) and ethylmercury (CH_3CH_2-Hg^+).[1] Therefore, detecting and monitoring mercury ions in the environment and food chain is crucial to prevent their harmful effects on human health and the ecosystem.

However, traditional detection methods for mercury ions, such as atomic absorption spectroscopy (AAS), atomic emission spectrometry (AES), electrochemistry, and inductively coupled plasma-atomic emission spectroscopy (ICP-OES), require sophisticated and time-consuming pretreatment and equipment, making real-time onsite detection challenging.[2–7] To overcome these limitations, fluorescent probes have emerged as a simple and cost-effective detection method with high sensitivity and selectivity, real-time monitoring capabilities, and easy procedures.[8] Fluorescent probes have found applications in various fields, including environmental monitoring, food safety, live cell imaging, and medical diagnosis.[9]

To date, many fluorescent probes based on various fluorophores have been developed for the detection of mercury ions *in vitro* and *in vivo*.[10–15] Among of them, rhodamine-based fluorophore has been widely used due to its commercial available, good photostability, relatively long absorption and emission wavelengths and simple structural derivatization.[16–30] Rhodamine derivatives exhibit very weak fluorescence in the spirocyclic form and strong fluorescence in the ring-opening form, triggered by specific analyte chelation. Hence, a new fluorescent probe, **RHOQ**, was developed for highly selective Hg^{2+} detection based on the ring close/opening transformation of the rhodamine platform (Scheme 1). Compared with recently reported fluorescent probe for Hg^{2+} (Table S1†), probe **RHOQ** demonstrated faster response, lower detection limit and higher fluorescence enhancement ratio. Furthermore, **RHOQ** can successfully monitor Hg^{2+} in living HeLa cells with low cytotoxicity.

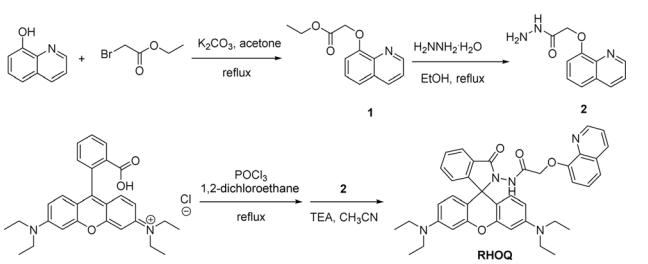

Scheme 1 Synthetic route of probe **RHOQ**.

[a]*Department of Biology, Xinzhou Normal University, Xinzhou, Shanxi Province 034000, P. R. China*

[b]*Shanxi Weipu Testing Technology Co. Ltd, Taiyuan, Shanxi Province 030012, P. R. China*

[c]*Department of Chemical and Biological Engineering, Hong Kong University of Science and Technology, Clear Water Bay Road, Saikung, Hong Kong SAR, Hong Kong. E-mail: qihuayou@ust.hk*

† Electronic supplementary information (ESI) available. See DOI: https://doi.org/10.1039/d4ra06115b

2 Experimental

2.1 Reagents and instrumentation

High-purity solvents and chemicals were purchased from Sigma-Aldrich Inc. with analytical grade. Metal ions including Ag^+, Li^+, Ca^{2+}, Co^{2+}, Cu^{2+}, Fe^{2+}, Hg^{2+}, Ni^{2+}, Pb^{2+}, Zn^{2+}, and Fe^{3+} were purchased as perchlorates, K^+, Na^+, and Mg^{2+} were purchased as chlorides.

Bruker Avance-III 400 MHz spectrometer was used to collect ^{1}H-NMR and ^{13}C-NMR spectra with TMS internal reference at 400 and 100 MHz, respectively. Bruker Autoflex mass spectrometer (MALDI-TOF) was used to record high-resolution mass spectrum (HRMS). PerkinElmer LS50B (Waltham, MA, USA) and Cary UV-300 spectrometer were used to collect fluorescence spectra and UV-Vis spectra, respectively. Orion 420A pH/mV/temperature benchtop meter was used for pH measurements.

2.2 Synthesis of probe RHOQ

Compound 1. A mixture of 8-hydroxyquinoline (1.60 g, 11 mmol), ethyl bromoacetate (1.93 g, 15.5 mmol) and K_2CO_3 (3.3 g, 24 mmol) in acetone (50 mL) was heated to reflux for 30 hours. After cooling, solid was filtered off and washed with small portions of ethyl acetate. The filtrates were combined and evaporated to dryness. The residue was purified by column chromatography on silica gel (PE : EA = 1 : 1) to give compound **1** (2.42 g, 95%) as a yellow oil. ^{1}H-NMR (400 MHz, $CDCl_3$) δ (ppm): 8.96 (1H, dd, J = 4.1 Hz, J = 1.7 Hz), 8.15 (1H, dd, J = 8.3 Hz, J = 1.7 Hz), 7.47–7.41 (3H, m), 6.97 (1H, dd, J = 6.7 Hz, J = 2.2 Hz), 4.98 (2H, s), 4.28 (2H, q, J = 7.3 Hz), 1.27 (3H, t, J = 7.3 Hz). ^{13}C-NMR (100 MHz, $CDCl_3$) δ (ppm): 168.83, 153.68, 149.57, 140.18, 135.93, 129.57, 126.36, 121.82, 120.90, 109.39, 66.19, 61.42, 14.18.

Compound 2. To a solution of compound **1** (1.5 g, 6.5 mmol) in EtOH (30 mL) was added hydrazine monohydrate (3 mL) in one portion and the reaction mixture was heated to reflux for 3 hours. After cooling, solvent was removed under reduced pressure, the solid was washed with small portions of water and EtOH and dried to give compound **2** (1.2 g, 85%) as a white solid. ^{1}H-NMR (400 MHz, DMSO-*d*6) δ (ppm): 9.55 (1H, s), 8.88 (1H, dd, J = 4.1 Hz, J = 1.6 Hz), 8.35 (1H, dd, J = 8.3 Hz, J = 1.4 Hz), 7.58–7.49 (3H, m), 7.23 (1H, dd, J = 7.7 Hz, J = 1.3 Hz), 4.74 (2H, s), 4.40 (2H, s). ^{13}C-NMR (100 MHz, DMSO-*d*6) δ (ppm): 166.79, 153.76, 149.29, 139.64, 136.07, 129.06, 126.75, 122.00, 120.84, 111.42, 68.07.

Probe RHOQ. To a suspension of rhodamine B (0.5 g, 1.0 mmol) in 1,2-dichloroethane (10 mL) was added $POCl_3$ (0.4 mL, 4.4 mmol) dropwise over 2 min under N_2 atmosphere and the reaction mixture was refluxed for 4 hours. The mixture was then cooled and evaporated *in vacuo*, the residue was dissolved in CH_3CN (80 mL) and this acid chloride solution was added dropwise to a solution of compound **2** (0.23 g, 1.0 mmol) and TEA (0.5 mL) in CH_3CN (20 mL) over 1 hour at room temperature. The reaction mixture was then refluxed for 2 hours. After solvent was evaporated under reduced pressure, the crude product was purified by column chromatography on silica gel (PE : EA = 1 : 5) to give compound **RHOQ** (420 mg, 65%) as a white solid. ^{1}H-NMR (400 MHz, CD_3CN) δ (ppm): 10.78 (1H, br. s), 8.23–8.14 (m, 2H), 7.87–7.85 (m, 1H), 7.61–7.48 (m, 4H), 7.28–7.20 (m, 2H), 7.04–7.02 (m, 1H), 6.59–6.58 (m, 2H), 6.32–6.24 (m, 4H), 4.65 (s, 2H), 3.33 (q, J = 6.9 Hz, 8H), 1.11 (t, J = 7.0 Hz, 12H). ^{13}C-NMR (100 MHz, CD_3CN) δ (ppm): 167.00, 163.52, 154.22, 153.34, 151.77, 148.60, 135.80, 132.85, 129.28, 128.95, 128.13, 126.55, 123.45, 122.40, 121.40, 107.37, 104.12, 96.78, 65.28, 43.62, 11.56. HRMS (ESI): m/z [M + H$^+$] calcd for $C_{39}H_{40}N_5O_4^+$: 641.3002; found: 642.3053; m/z [M + Na$^+$] calcd for $C_{39}H_{39}N_5O_4Na^+$: 664.2894; found: 664.1235; m/z [M + K$^+$] calcd for $C_{39}H_{39}N_5O_4K^+$: 680.2634; found: 679.9705.

2.3 Spectroscopic measurements

Various cation solutions including LiCl, NaCl, KCl, $CaCl_2$, $MgCl_2$ (100 mM), and $AgClO_4 \cdot H_2O$, $Cd(ClO_4)_2 \cdot 6H_2O$, $Co(ClO_4)_2 \cdot 6H_2O$, $Cu(ClO_4)_2 \cdot 6H_2O$, $Fe(ClO_4)_2$, $Fe(ClO_4)_3$, $Hg(ClO_4)_2 \cdot 3H_2O$, $Ni(ClO_4)_2 \cdot 6H_2O$, $Pb(ClO_4)_2 \cdot 3H_2O$, $Zn(ClO_4)_2 \cdot 6H_2O$ (10 mM) were prepared in double-distilled water. Probe **RHOQ** was dissolved in MeOH to prepare 1.0 mM stock solution. All the absorption and fluorescence spectra measurements were conducted in MeOH–H_2O solution (1 : 9, v/v, 40 mM HEPES, pH 7.4). In the fluorescence experiments, the excitation wavelength was set at 543 nm, and the excitation/emission slit widths were set at 5/5 nm, respectively.

2.4 Cytotoxicity assay

The cellular toxicity of probe **RHOQ** was tested by MTT assay. HeLa cells were seeded into 96 well plates at a density of 4000 cells per well at 37 °C with 5% CO_2 for 24 h, and then incubated with 0.1% DMSO and different concentration of probe solution (5, 10, 20, 30 μM), respectively. Subsequently, 20 μL of MTT solution was added to each well followed by incubation for an additional 4 h. The absorbance of each well was measured at 490 nm.

2.5 Cell culture and imaging

Probe **RHOQ** (1.0 mM) was prepared in DMSO solution. HeLa cells were cultured in Minimum Essential Medium (MEM) with 10% fetal bovine serum (FBS) and 1% antibiotics at 37 °C in an atmosphere of 5% CO_2 and 95% humidity. The HeLa cells were plated on coverslips and washed 3 times with phosphate buffered saline (PBS) followed by incubating with the probe solution (10 μM) in DMSO for 30 min at 37 °C, and then washed with PBS three times. After incubating with $Hg(ClO_4)_2$ solution (10 μM) in PBS for 30 min at 37 °C, the cells were washed with PBS three times again.

3 Results and discussion

3.1 The synthesis of RHOQ

The synthetic route of probe **RHOQ** was outlined in Scheme 1. Intermediate **1** was obtained by reacting 8-hydroxyquinoline with ethyl bromoacetate with a high yield. Subsequently, the reaction of **1** with hydrazine under reflux conditions gave compound **2** with an easy work-up operation. Finally, the condensation of rhodamine B with compound **2** in CH_3CN yielded the target probe **RHOQ**. All chemical structures were

confirmed by ^{1}H and ^{13}C NMR spectroscopy, as well as high resolution mass spectroscopy (detailed in the Experimental section and ESI†).

3.2 Selectivity of RHOQ

After the synthesis of the probe, the selectivity of **RHOQ** (10 μM) towards various metal ions, including Na^{+}, K^{+}, Li^{+}, Mg^{2+}, Ca^{2+}, Mg^{2+}, Ag^{+}, Cu^{2+}, Co^{2+}, Ni^{2+}, Cd^{2+}, Zn^{2+}, Hg^{2+}, Fe^{2+} and Fe^{3+}, was investigated in a MeOH–Tris buffer (20 mM, pH = 7.4, 1 : 9, v/v) solution using UV-Vis and fluorescence spectroscopy. The absorption spectrum of **RHOQ** exhibited negligible absorbance in the range from 400 to 700 nm because **RHOQ** mainly exists in spirolactam form. Upon the addition of Hg^{2+}, a strong absorption peak at 566 nm with a characteristic broad shoulder band centered at about 521 nm appeared (Fig. 1), suggesting the conversion of the spirolactam form to the ring-opening amide form of **RHOQ**. As shown in the inset of Fig. 1, the addition of Hg^{2+} to the solution of **RHOQ** induced a prominent colour changed from colourless to magenta. In addition, similar phenomenon was also observed upon the addition of Cu^{2+}, while other metal ions did not trigger any changes. In the fluorescence experiments, the addition of Hg^{2+} induced a significant fluorescence enhancement (550-fold) at 594 nm, while Fe^{3+} caused a relatively small fluorescence change (15-fold) with a small hypsochromic shift (fluorescence maximum at 584 nm), and other metal ions induced negligible changes (Fig. 2). Consistent with the results of fluorescent experiments, only the addition of Hg^{2+} to the solution of **RHOQ** can emit distinct red fluorescence under the irradiation of UV lamp (inset of Fig. 2).

3.3 Interference effect of RHOQ

After investigating the selectivity of **RHOQ** for various cations, the potential interference effect of other cations on the selectivity of **RHOQ** for Hg^{2+} detection was examined. As shown in Fig. 3, the presence of high concentrations of various cations (40 equiv.) did not interfere with Hg^{2+} detection of **RHOQ**. Especially, the presence of Cu^{2+}, known as a paramagnetic fluorescence quencher, did not affect the detection of Hg^{2+} by the **RHOQ**. Similarly, absorbance measurements also showed no significant changes in the presence of various competing ions (Fig. S8†). These results confirmed that **RHOQ** has a highly potential application in the detection of Hg^{2+} in living organisms. The selectivity and interference effect of **RHOQ** for Hg^{2+} detection was confirmed, indicating its potential application in detecting Hg^{2+} in living organisms.

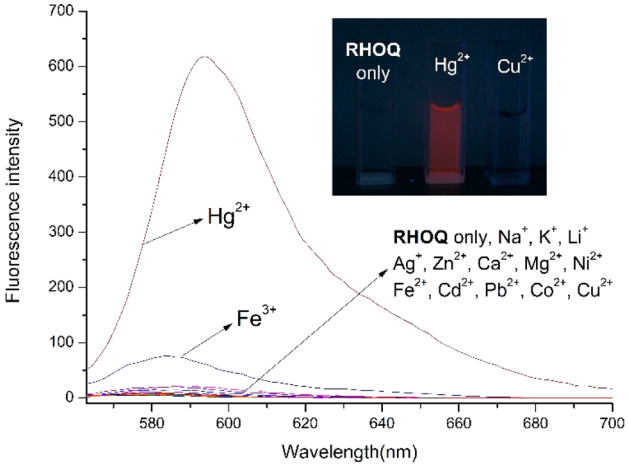

Fig. 2 Fluorescence spectrum of **RHOQ** (10 μM) upon addition of different metal ions in MeOH–Tris buffer (20 mM, pH = 7.4, 1 : 9, v/v). Inset: visible emission of **RHOQ** observed under a UV lamp in the absence (left) and presence of Hg^{2+} (middle) or Cu^{2+} (right).

3.4 Titration experiments of RHOQ

Additionally, UV/Vis and fluorescence titration of **RHOQ** in MeOH–Tris buffer (20 mM, pH = 7.4, 1 : 9, v/v) upon the

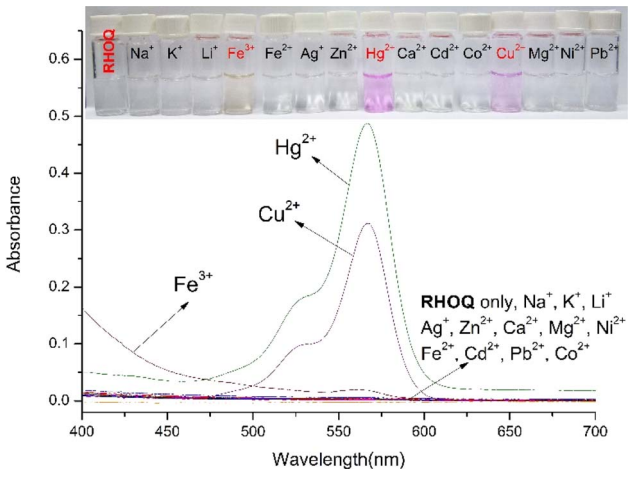

Fig. 1 Absorption spectrum of **RHOQ** (10 μM) upon addition of different metal ions in MeOH–Tris buffer (20 mM, pH = 7.4, 1 : 9, v/v). Inset: visual color change of **RHOQ** upon addition of different metal ions.

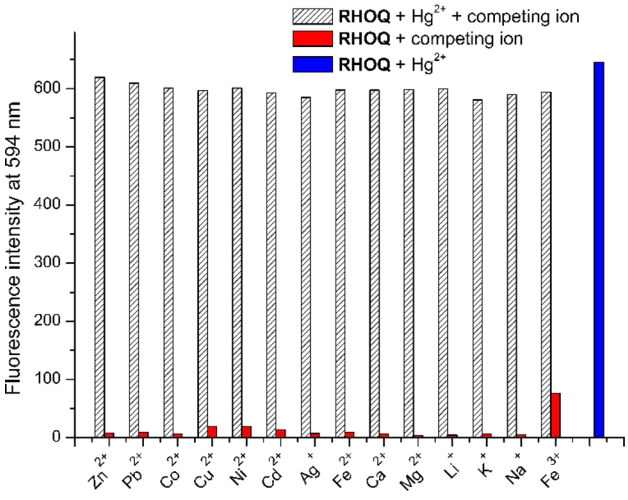

Fig. 3 Change of fluorescence intensity at 594 nm of **RHOQ** (10 μM) in MeOH–Tris buffer (20 mM, pH = 7.4, 1 : 9, v/v) upon addition of competing metal ions (40 equiv.) in the absence (black) and presence (red) of Hg^{2+} (40 equiv.).

addition of Hg^{2+} were conducted. After the addition of Hg^{2+} (40 equiv.), the binding of **RHOQ** with Hg^{2+} reached equilibrium, as evidenced by both absorbance and fluorescence measurement. Nonlinear fitting of the titration curves using the Benesi–Hildebrand equation (eqn (1))[31,32] assuming a 1 : 1 stoichiometry for the **RHOQ**–Hg^{2+} complex yielded association constant K_{ass} of about 1.05×10^5 L mol^{-1} ($R^2 = 0.990$) and 9.18×10^3 L mol^{-1} ($R^2 = 0.990$) from UV/Vis (Fig. 4) and fluorescence (Fig. 5) titration, respectively.

$$\frac{1}{F - F_0} = \frac{1}{K(F_{max} - F_0)[Hg^{2+}]} + \frac{1}{F_{max} - F_0} \quad (1)$$

where F_0 is the absorbance or fluorescence intensity of **RHOQ**, F is the absorbance or fluorescence intensity of **RHOQ**–Hg^{2+} complex, F_{max} is the absorbance or fluorescence intensity of **RHOQ** with excess amount of Hg^{2+}, K is the association constant (L mol^{-1}), and $[Hg^{2+}]$ is the concentration of Hg^{2+} (mol L^{-1}). According to the fluorescence titration experiment, a linear fluorescence intensity enhancement was observed in the range of 0–120 μM of Hg^{2+} with a calculated limit of detection (LOD = $3\sigma/K$) of 9.67×10^{-8} M (Fig. S9†).[33–35] Therefore, probe **RHOQ** could be utilized as a promising method for the sensitive and quantitative detection of Hg^{2+} in an aqueous solution.

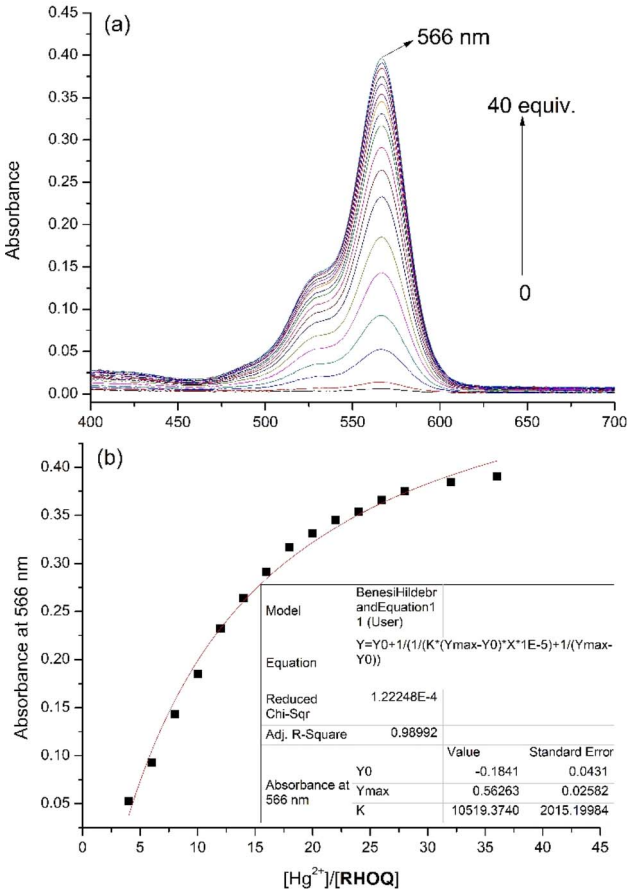

Fig. 4 (a) Absorption spectra of **RHOQ** (10 μM) upon addition of Hg^{2+} in MeOH–Tris buffer (20 mM, pH = 7.4, 1 : 9, v/v). (b) Absorbance at 566 nm of **RHOQ** as a function of Hg^{2+} concentration (0–40 equiv.).

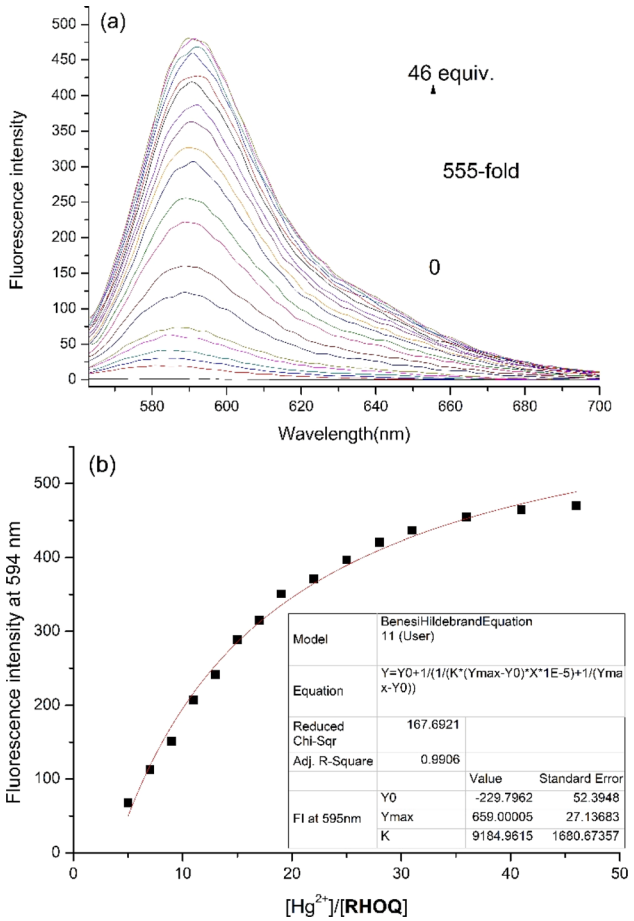

Fig. 5 (a) Fluorescence spectra of **RHOQ** (10 μM) upon addition of Hg^{2+} in MeOH–Tris buffer (20 mM, pH = 7.4, 1 : 9, v/v). (b) Fluorescence intensity at 594 nm of **RHOQ** as a function of Hg^{2+} concentration (0–40 equiv.).

3.5 pH effect of RHOQ

The pH-dependent emission measurements revealed that **RHOQ** exhibited high stability and non-fluorescence in the pH range from 4.0–10.0 (Fig. 6). A slight fluorescence enhancement of **RHOQ** below pH 4.0 may be attributed to the well-known spirolactam ring opening in strong acidic condition. On the other hand, the addition of Hg^{2+} to the solution of **RHOQ** induced a significant fluorescence enhancement in acidic or weak alkaline conditions (pH < 8.0), while a dramatic decrease in fluorescence intensity was observed at pH higher than 8.2. This result may be ascribed to the formation of insoluble $Hg(OH)_2$ in alkaline conditions, leading to the conversion of the ring-opening **RHOQ**–Hg^{2+} complex back to the original spirolactam compound. These findings support the suitability of **RHOQ** for the detection of Hg^{2+} in living cells.

3.6 Reversibility and time-dependent response of RHOQ

The reversibility of probe for metal ion detection is a crucial characteristic for practical applications. To test the reversibility of **RHOQ**, an aqueous solution of Na_2EDTA (disodium ethylenediaminetetraacetate) was introduced to the solution of

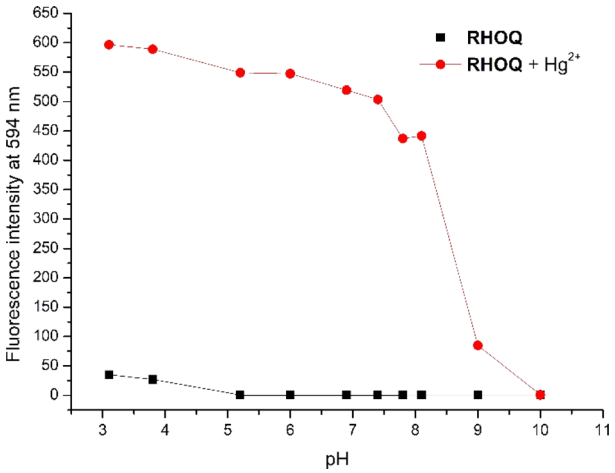

Fig. 6 Plot of fluorescence intensity at 594 nm of **RHOQ** (10 μM) in MeOH–Tris buffer (20 mM, 1 : 9, v/v) in the presence (red dot) and absence (black square) of Hg^{2+} (40 equiv.) as a function of pH.

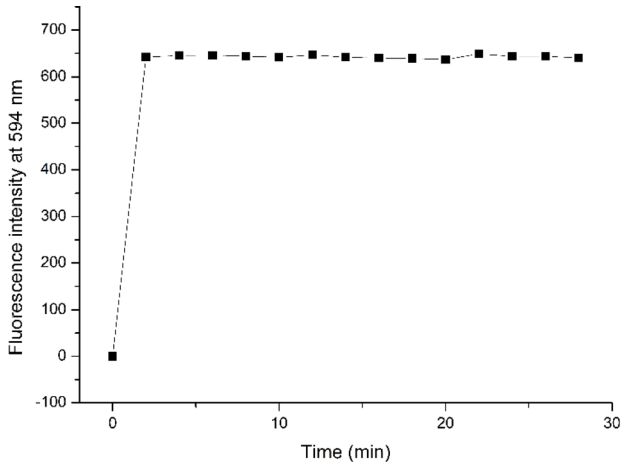

Fig. 8 Time-dependent fluorescence intensity at 594 nm of **RHOQ** (10 μM) in MeOH–Tris buffer (20 mM, pH = 7.4, 1 : 9, v/v) upon the addition of Hg^{2+} (40 equiv.).

RHOQ (10 μM) and Hg^{2+} (Fig. 7). The fluorescence intensity of **RHOQ**–Hg^{2+} complex decreased significantly and approached the original intensity of **RHOQ**. These outcomes can also be attributed to the spirolactam ring opening/closing interconversion, which aligns with the findings obtained from the pH-dependent experiments.

We also investigated the time-dependent responses of **RHOQ** to Hg^{2+} (Fig. 8). Upon the addition of Hg^{2+}, the solution of **RHOQ** showed an instantaneous color change to red, with stable maximum fluorescence intensity for at least 30 minutes, demonstrating the suitability of **RHOQ** for real-time Hg^{2+} detection.

3.7 Binding mode of RHOQ and Hg^{2+}

To elucidate the possible binding mode between **RHOQ** and Hg^{2+}, Job's plot experiments were conducted using fluorescent method. The result clearly indicated that the maximum fluorescence intensity was located at a mole fraction around 0.5 for Hg^{2+} (Fig. 9), confirming a 1 : 1 binding stoichiometry between **RHOQ** and Hg^{2+}. This result is consistent with the non-linear fitting of titration curve using the Benesi–Hildebrand equation. In order to investigate the binding mode of **RHOQ** and Hg^{2+}, ^1H NMR titration experiments were conducted. Upon addition of solution of $Hg(ClO_4)_2$ in D_2O to the solution of **RHOQ** in CD_3CN, the proton peaks corresponding to H_a, H_b and H_c shifted to lower field (Fig. 10). This observation implied that Hg^{2+} coordinated with N atom on quinoline group and O atom on carbonyl group (–$COCH_2O$–). According to these results, we proposed a possible fluorescence OFF–ON mechanism of **RHOQ** upon addition of Hg^{2+}, Fe^{3+} and Cu^{2+}, respectively (Scheme 2). As we know, rhodamine B or its derivatives generally exist in five-membered spirolactam form with non-fluorescent behaviour. While in the presence of specific metal cations, the coordination of metal cation with oxygen atom on the spirolactam

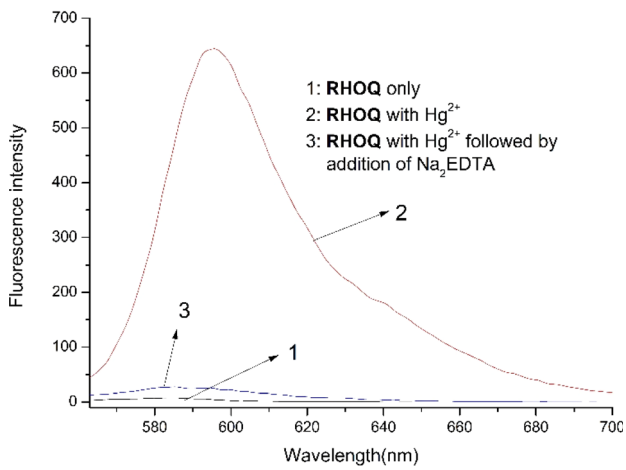

Fig. 7 Fluorescence spectra of **RHOQ** (10 μM) upon addition of Hg^{2+} (40 equiv.) followed by the addition of Na_2EDTA in MeOH–Tris buffer (20 mM, pH = 7.4, 1 : 9, v/v).

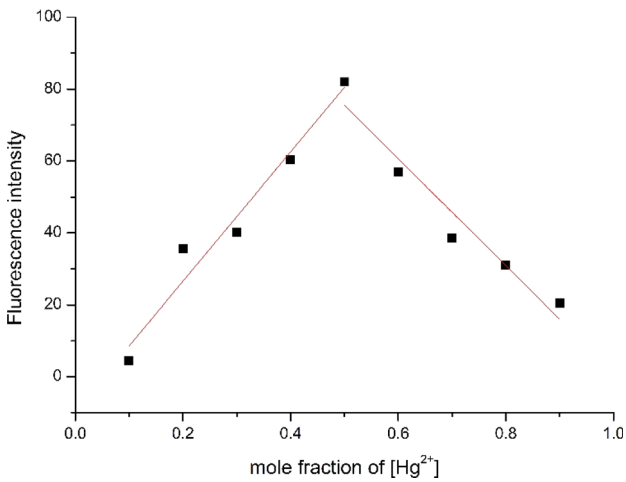

Fig. 9 Job's plot by fluorescence method of the complex between **RHOQ** and Hg^{2+} in MeOH–Tris buffer (20 mM, pH = 7.4, 1 : 9, v/v). Total concentration of **RHOQ** and Hg^{2+} is 50 μM.

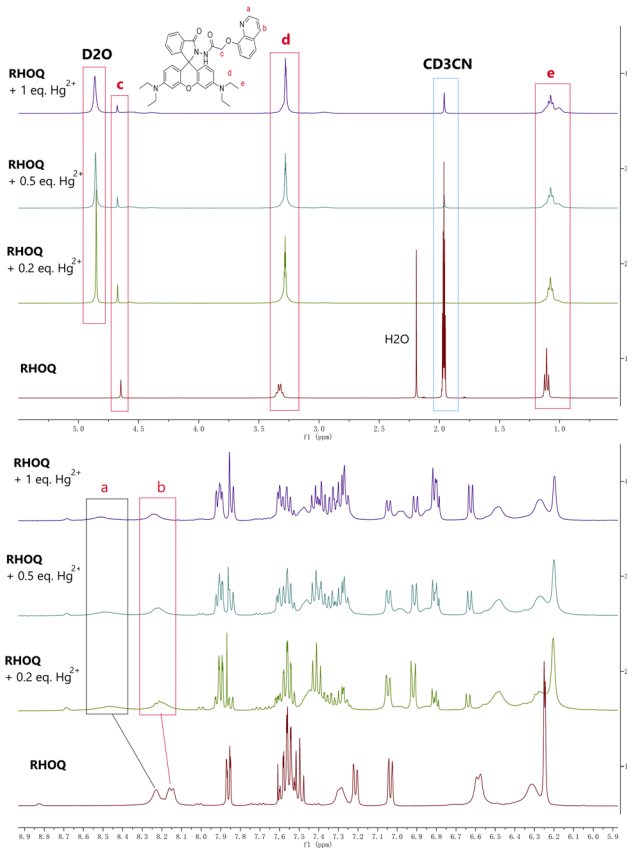

Fig. 10 ^{1}H NMR spectra corresponding to the titration of **RHOQ** in CD_3CN with $Hg(ClO_4)_2$ in D_2O.

moiety of rhodamine B derivatives triggers the opening of spirolactam form to give a strong red fluorescence. To the probe **RHOQ**, the introduction of another amide group and 8-hydroxyquinoline moiety provides specific coordination sites for Hg^{2+}, thus the selectivity of probe **RHOQ** to Hg^{2+} was enhanced.

Additionally, when Cu^{2+} was added to **RHOQ** solution, we observed an absorption spectrum similar to that of Hg^{2+}, but no fluorescence was produced (Fig. 1 and 2). This phenomenon can be attributed to the relatively high binding affinity of Cu^{2+} for **RHOQ** and its well-known paramagnetic nature.[36,37] Fortunately, the high concentration of Cu^{2+} did not interfere with the

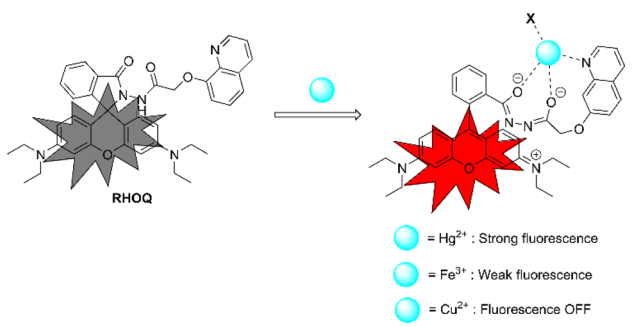

Scheme 2 Proposed binding mechanism of **RHOQ** upon addition of Hg^{2+}, Fe^{3+} and Cu^{2+}, respectively. (X = coordinating anion or solvent).

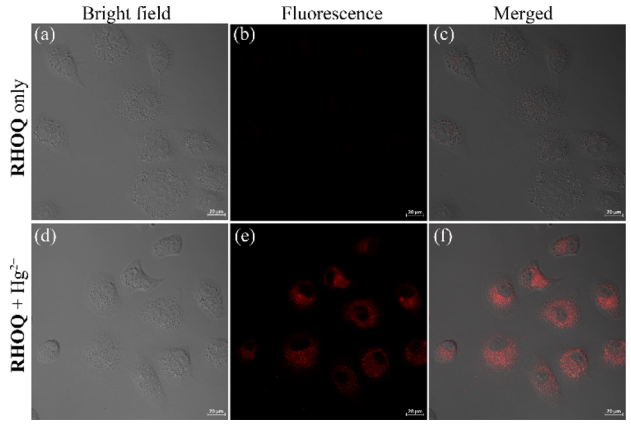

Fig. 11 Confocal microscopy images of HeLa cell staining with **RHOQ** (10 μM) (a–c) followed by the incubation of Hg^{2+} (10 μM) (d–f). (a) and (d) bright field images; (b) and (e) fluorescence images collected in the range of 580–640 nm; (c) overlay of (a) and (b); (f) overlay of (d) and (e).

sensing of Hg^{2+} by **RHOQ**. Due to the higher binding affinity of Hg^{2+} for **RHOQ** compared to Cu^{2+}, Hg^{2+} would replace Cu^{2+} in the **RHOQ**–Cu^{2+} complex to form a new **RHOQ**–Hg^{2+} complex, thereby regenerating the fluorescence. Similarly, the much lower binding affinity of Fe^{3+} for **RHOQ** resulted in significantly low absorbance and fluorescence intensity.

3.8 Cytotoxicity and bioimaging application of RHOQ

Building on the above experimental results, further studies were conducted in biological environments using HeLa cells. The cytotoxicity of **RHOQ** was evaluated using MTT assays before cell imaging (Fig. S10†). Living HeLa cells were incubated with different concentrations of probe **RHOQ** (0–30 μM) for 24 h at 37 °C, and the results suggested that the cell viability had negligible change, which indicated that **RHOQ** was low cytotoxicity to living cells.

To test the capability of **RHOQ** to detection Hg^{2+} in living cells, HeLa cells were incubated with probe **RHOQ** (10 μM) at 37 °C for 30 min. Negligible fluorescence was found in the range of 580–640 nm (Fig. 11a–c). Upon further incubation of $Hg(ClO_4)_2$ for 30 min, a strong red fluorescence was observed (Fig. 11d–f), indicating that the intracellular uptake of Hg^{2+} resulted the spirolactam ring opening of **RHOQ** and fluorescence enhancement. These results showed that **RHOQ** has good cell membrane permeability and can be utilized for the detection of Hg^{2+} in living cells.

4 Conclusions

In summary, a highly Hg^{2+}-selective rhodamine-based turn-on fluorescent probe **RHOQ**, was designed and investigated for Hg^{2+} detection. The probe exhibited a visual color change to Hg^{2+} and Cu^{2+}, while only the presence of Hg^{2+} triggers intense fluorescence enhancement of **RHOQ** due to the formation of spirolactam ring-opening form of **RHOQ**. Common alkali, alkali earth and transition metal ions did not cause any interference to the fluorescence detection of Hg^{2+}. With fast response, a wide

applicable pH range, and a low detection limit (9.67×10^{-8} M), **RHOQ** holds promise for the sensitive and quantitative detection of Hg^{2+} in aqueous solutions. Additionally, MTT assays confirmed that **RHOQ** has low cytotoxicity toward living cells and can be utilized for the detection of Hg^{2+} in living cells. These results manifest that **RHOQ** has a good application prospect in the detection of Hg^{2+}.

Data availability

The data supporting this article have been included as part of the ESI.†

Author contributions

Lei Zhang: investigation, formal analysis, resources, writing-original draft, funding acquisition. Jun Guo: investigation, formal analysis, resources. Qihua You: conceptualization, methodology, writing-review & editing, supervision.

Conflicts of interest

There are no conflicts to declare.

Acknowledgements

This work was supported by the Key R&D Program of Xinzhou Science and Technology Project (No. 20220301), and Scientific Research Project of Xinzhou Normal University (Grant No. 00001022).

Notes and references

1 P. A. Nogara, M. Farina, M. Aschner and J. B. T. Rocha, *Chem. Res. Toxicol.*, 2019, **32**, 1459–1461.
2 M. Zaib, M. M. Athar, A. Saeed and U. Farooq, *Biosens. Bioelectron.*, 2015, **74**, 895–908.
3 J. Sardans, F. Montes and J. Peñuelas, *Soil Sediment Contam.*, 2011, **20**, 447–491.
4 F. X. Han, W. D. Patterson, Y. Xia, B. B. M. Sridhar and Y. Su, *Water, Air, Soil Pollut.*, 2006, **170**, 161–171.
5 R. S. Reimers, W. D. Burrows and P. A. Krenkel, *J. - Water Pollut. Control Fed.*, 1973, **45**, 814–828.
6 N. Kallithrakas-Kontos and S. Foteinis, *Curr. Anal. Chem.*, 2016, **12**, 22–36.
7 H. Morita, H. Tanaka and S. Shimomura, *Spectrochim. Acta, Part B*, 1995, **50**, 69–84.
8 T. Samanta and R. Shunmugam, *Mater. Adv.*, 2021, **2**, 64–95.
9 M. Vendrell, D. Zhai, J. C. Er and Y.-T. Chang, *Chem. Rev.*, 2012, **112**, 4391–4420.
10 F. Bu, B. Zhao, W. Kan, L. Ding, T. Liu, L. Wang, B. Song, W. Wang and Q. Deng, *J. Photochem. Photobiol., A*, 2020, **387**, 112165.
11 H. Lv, G. Yuan, G. Zhang, Z. Ren, H. He, Q. Sun, X. Zhang and S. Wang, *Dyes Pigm.*, 2020, **172**, 107658.
12 S. Subedi, L. N. Neupane, H. Yu and K.-H. Lee, *Sens. Actuators, B*, 2021, **338**, 129814.
13 X. Wu, N. Duan, Y. Li, S. Yang, H. Tian and B. Sun, *J. Photochem. Photobiol., A*, 2020, **388**, 112209.
14 N. Xiao, H. Xu, Y. Liu, Y. Tian, R. Tan, Y. Peng and Y.-W. Wang, *Tetrahedron Lett.*, 2023, **120**, 154435.
15 Y. Yu, C. Liu, B. Tian, X. Cai, H. Zhu, P. Jia, Z. Li, X. Zhang, W. Sheng and B. Zhu, *Dyes Pigm.*, 2020, **177**, 108290.
16 B. Sen, M. Mukherjee, S. Pal, K. Dhara, S. K. Mandal, A. R. Khuda-Bukhsh and P. Chattopadhyay, *RSC Adv.*, 2014, **4**, 14919–14927.
17 S. O. Aderinto, Y. Xu, H. Peng, F. Wang, H. Wu and X. Fan, *J. Fluoresc.*, 2017, **27**, 79–87.
18 Y. Wang, H. Ding, S. Wang, C. Fan, Y. Tu, G. Liu and S. Pu, *RSC Adv.*, 2019, **9**, 11664–11669.
19 K. P. Carter, A. M. Young and A. E. Palmer, *Chem. Rev.*, 2014, **114**, 4564–4601.
20 D. Wu, M. Ma, M. Zhang, Y. Xiao, H. Yu, Y. Shao, X. Zhang, Z. Cheng and Y. Xiao, *Dyes Pigm.*, 2022, **198**, 110001.
21 H. Zhang, J. Song, S. Wang, Q. Song, H. Guo and Z. Li, *Dyes Pigm.*, 2023, **216**, 111380.
22 B. D. Vanjare, P. G. Mahajan, H.-I. Ryoo, N. C. Dige, N. G. Choi, Y. Han, S. J. Kim, C.-H. Kim and K. H. Lee, *Sens. Actuators, B*, 2021, **330**, 129308.
23 B. Du, Q. Li, K. Huang and L. Liang, *J. Mol. Struct.*, 2023, **1271**, 134015.
24 K. Huang, Y. Liu, Q. Li, B. Yu, L. Liang and D. Qin, *Spectrochim. Acta, Part A*, 2022, **281**, 121651.
25 Y. Zhao, Y. Sun, X. Lv, Y. Liu, M. Chen and W. Guo, *Org. Biomol. Chem.*, 2010, **8**, 4143–4147.
26 B. Du, Q. Li, K. Huang, Q. Wang and L. Liang, *J. Photochem. Photobiol., A*, 2023, **436**, 114419.
27 Y. Wang, H. Ding, S. Wang, C. Fan, Y. Tu, G. Liu and S. Pu, *RSC Adv.*, 2019, **9**, 11664–11669.
28 Z.-Q. Xu, X.-J. Mao, Y. Wang, W.-N. Wu, P.-D. Mao, X.-L. Zhao, Y.-C. Fan and H.-J. Li, *RSC Adv.*, 2017, **7**, 42312–42319.
29 C. Kan, X. Wang, L. Wu, X. Shao, H. Xing, M. You and J. Zhu, *Anal. Methods*, 2021, **13**, 3987–3993.
30 B. Li, F. Tian and Y. Hua, *RSC Adv.*, 2022, **12**, 21129–21134.
31 Y. Shiraishi, S. Sumiya, Y. Kohno and T. Hirai, *J. Org. Chem.*, 2008, **73**, 8571–8574.
32 Q.-H. You, H.-B. Huang, Z.-X. Zhuang, X.-R. Wang and W.-H. Chan, *Bull. Korean Chem. Soc.*, 2016, **37**, 1772–1777.
33 J. M. An, S. Kang, E. Huh, Y. Kim, D. Lee, H. Jo, J. F. Joung, V. J. Kim, J. Y. Lee, Y. S. Dho, Y. Jung, J. K. Hur, C. Park, J. Jung, Y. Huh, J.-L. Ku, S. Kim, T. Chowdhury, S. Park, J. S. Kang, M. S. Oh, C.-K. Park and D. Kim, *Chem. Sci.*, 2020, **11**, 5658–5668.
34 Q.-H. You, P.-S. Chan, W.-H. Chan, S. C. K. Hau, A. W. M. Lee, N. K. Mak, T. C. W. Mak and R. N. S. Wong, *RSC Adv.*, 2012, **2**, 11078–11083.
35 G. Bao, B. Zhou and Y. Han, *Tetrahedron Lett.*, 2022, **100**, 153887.
36 Q.-H. You, P.-S. Chan, W.-H. Chan, S. C. K. Hau, A. W. M. Lee, N. K. Mak, T. C. W. Mak and R. N. S. Wong, *RSC Adv.*, 2012, **2**, 11078–11083.
37 N. Kumari, N. Dey and S. Bhattacharya, *RSC Adv.*, 2014, **4**, 4230–4238.